IET Generation, Transmission & Distribution

Special Issue: Emerging Technologies for Virtual Power Plant and Microgrid

IET Journals
The Institution of Engineering and Technology

Stackelberg game-based energy management for a microgrid with commercial buildings considering correlated weather uncertainties

ISSN 1751-8687
Received on 30th May 2018
Revised 3rd October 2018
Accepted on 15th November 2018
E-First on 26th March 2019
doi: 10.1049/iet-gtd.2018.5743
www.ietdl.org

Jiaying Wang[1], Changsen Feng[1], Yan Xu[2], Fushuan Wen[1] ✉, Lijun Zhang[3], Chengbo Xu[3], Abdus Salam[4]

[1]*School of Electrical Engineering, Zhejiang University, Hangzhou 310027, People's Republic of China*
[2]*School of Electrical & Electronic Engineering, Nanyang Technological University, Singapore 639798, Singapore*
[3]*State Grid Zhejiang Economic Research Institute, Hangzhou 310008, People's Republic of China*
[4]*Department of Electrical and Electronic Engineering, Universiti Teknologi Brunei, Bandar Seri Begawan BE1410, Brunei*
✉ *E-mail: fushuan.wen@gmail.com*

Abstract: This paper proposes a Stackelberg game-based optimal energy management model for a microgrid with commercial buildings (CBs), which include a cluster of flexible loads, such as a heating, ventilation, and air conditioning (HVAC) system and a lighting system. In particular, the microgrid operator (MGO) determines the optimal energy management scheme while the CBs enjoy a dynamic pricing tariff to adjust their consumption patterns for cost saving. The interactions between MGO and CBs are formulated as a bi-level optimisation problem where the MGO behaves as a leader and CBs act as followers. The proposed model is transformed into a mixed integer linear programming (MILP) problem by jointly using the Karush–Kuhn–Tucker (KKT) condition and the strong duality theory. Besides, the effects of correlated solar irradiance and solar illuminance uncertainties on the load profile are taken into account through invoking the Nataf transformation-based $2\boldsymbol{M}+1$ point estimate method (PEM). Finally, case studies are served for demonstrating the feasibility and efficiency of the proposed method.

Nomenclatures

A. abbreviations

MGO	Microgrid operator
KKT	Karush–Kuhn–Tucker
ISO	Independent system operator
HVAC	Heating, ventilation and air conditioning
RTP	Real time price
TOU	Time-of-use
IAQ	Indoor air quality
PV	Photovoltaic
ESS	electric storage system
AHU	Air Handling Unit
VAV	Variable Air Volume
VFD	Variable Frequency Drive
PEM	Point estimate method
CDF	Cumulative distribution function
MILP	Mixed integer linear programming
DR	Demand response
DRM	Demand response management
CB	Commercial building

B. parameters

η_{cha}/η_{dis}	charge/discharge efficiency of ESS
$\mathrm{p}_{\mathrm{cha}}^{\max}/\mathrm{p}_{\mathrm{dis}}^{\max}$	maximum charge/discharge power of ESS, [kW]
$S_{\max}/S_{\min}$	maximum/Minimum storage energy in ESS, [kWh]
N_{cb}	number of commercial buildings in the microgrid
N	number of zones in a commercial building
ρ_t^{ws}	wholesale electricity price in period t, [¢ /kW]
$\rho_{\mathrm{t}}^{\max}/\rho_{\mathrm{t}}^{\min}$	maximum/Minimum retail electricity price in period t, [¢ /kW]
$\rho_{\mathrm{ave}}^{\mathrm{in}}$	upper bound of average retail electricity price, [¢ /kW]
$P_{\max}^{\mathrm{ws}}$	maximum trading power with the wholesale market, [kW]
$\tau_{\mathrm{sol}}^{\mathrm{ele}}$	photoelectric conversion efficiency of each PV panel
A_{ele}	area of each PV panel, [m^2]
E_{t}	solar irradiance in period t, [kW].
c_{air}	specific heat capacity of air, [J/(kg·K)].
ρ_{air}	air density, [$\mathrm{kg/m}^3$].
V^{i}	volume of the ith zone, [m^3]
B^{i}	heat transfer coefficient of ith zone
θ_t^{out}	outdoor temperature in period t, [℃]
$Q_{\mathrm{solar},t}^{i}$	solar radiation heat power for the ith zone in period t, [kW]
$Q_{\mathrm{infle},t}^{i}$	inflexible loads heat dissipation power in the ith zone during period t, [kW]
$\mathrm{Q}_{\mathrm{crowd,t}}^{\mathrm{i}}$	crowd heat dissipation power in the ith zone during period t, [kW]
F_{win}^{i}	area of windows in the ith zone, [m^2]
S_{she}^{i}	shading coefficient of the ith zone
λ_{light}	coefficient of heat dissipation of the lighting system
λ_{infle}	coefficient of heat dissipation of inflexible loads
$n_{\mathrm{crowd},t}^{i}$	number of people in the ith zone during period t
φ	clustering coefficient of the crowd
k	cooling load coefficient for sensible heat from human bodies
q_{sen}	sensible heat power from human bodies
q_{lat}	latent heat power from human bodies
$C_{\mathrm{crowd,t}}^{i}$	carbon dioxide generation by the crowd in the ith zone, [L/s]
C_t^{out}	outside carbon dioxide concentration, [ppm]
$\theta_{\max}/\theta_{\min}$	maximum/minimum allowable indoor temperature, [℃]
$C_{\max}/C_{\min}$	maximum/minimum allowable indoor carbon dioxide concentration, [ppm].
η	the efficiency factor of the cooling coil
COP	performance coefficient of the chiller
$\mathrm{k}_2/\mathrm{k}_1/\mathrm{k}_0$	coefficients related to fan power consumption
$m_{\mathrm{HVAC}}^{\max}/m_{\mathrm{HVAC}}^{\min}$	maximum/minimum HVAC air flow rate in each zone, [kg/s]
$M_{\mathrm{HVAC}}^{\max}$	maximum total HVAC air flow rate, [kg/s]

$\theta_{\max}^{\text{cool}}/\theta_{\min}^{\text{cool}}$	maximum/minimum cooling coil temperature, [℃]
$IL_{\text{out},t}$	outdoor solar illumination in period t, [lux]
$IL_{\max}/IL_{\min}$	maximum/minimum required inside illumination, [lux]
R_{light}	unit power consumption of the artificial lighting, [kW]
F_{in}^{i}	internal area in the ith zone, [m^2]
$P_{\max}^{\text{in}}$	maximum trading power between the microgrid and commercial buildings, [kW]

C. variables

S_{t}	state of Charge of ESS in period t, [kWh]
$P_{\text{cha},t}/P_{\text{dis},t}$	charge/discharge power of ESS in period t, [kW]
$x_{\text{cha},t}$	binary variable representing charging or discharging for ESS in period t (1 for charging, 0 for discharging)
ρ_t^{in}	retail electricity price in period t, [¢ /kW]
P_t^{in}	the total load power of each building in period t, [kW]
P_t^{ws}	purchasing power from the wholesale market in period t, [kW]
$P_{\text{sol},t}$	PV power in period t, [kW]
θ_t^{i}	indoor temperature of the ith zone in period t, [℃]
θ_t^{cool}	cooling coil temperature in period t, [℃]
θ_t^{mix}	mixed air temperature in period t, [℃]
$Q_{\text{light},t}^{i}$	lighting load heat dissipation power for the ith zone in period t, [kW]
$P_{\text{light},t}^{i}$	lighting power for the ith zone in period t, [kW]
$P_{\text{infle},t}^{i}$	inflexible loads power of the ith zone in period t, [kW]
C_t^{i}	carbon dioxide concentration in the ith zone during period t, [ppm]
C_t^{mix}	mixed carbon dioxide concentration supplied to each zone during period t, [ppm]
$P_{\text{HVAC},t}$	HVAC power in period t, [kW]
$P_{coil,t}$	cooling coil power in period t, [kW]
$P_{fan,t}$	VFD fan power in period t, [kW]
$m_{\text{HVAC},t}^{i}$	HVAC air flow rate of the ith zone in period t, [kg/s]
$IL_{\text{in},t}^{i}$	indoor lighting illumination in the ith zone during period t, [lux]

1 Introduction

1.1 Motivation and incitement

A microgrid, primarily including loads, renewable energy sources, and electric storage systems (ESSs), is often placed near the load centre [1]. With the rapid development of communications and control technologies, the microgrid operator (MGO) can respond immediately to electricity prices and schedule the controllable resources for potential benefits [2]. Therefore, how to determine the price-based demand response (DR) strategies and the optimal energy management for the microgrid has been a hot topic in both academic and industrial communities.

A two-level market structure is usually employed in a microgrid energy management in existing publications, in which the MGO is regarded as a central control agent that executes DR programs and negotiates on behalf of the consumers with the independent system operator (ISO) efficiently [3, 4]. With the implementation of the retail electricity market, the MGO would function as an intermediary agent between the ISO and consumers. Specifically, the MGO determines the energy procurement from the wholesale electricity market and sells electricity to consumers in turn at a retail price, which induces consumers to adjust their consumption patterns effectively and thus acts as a key factor in an energy management model for a microgrid. Ordinarily, the retail price model includes real-time pricing, time-of-use (TOU) pricing, critical peak pricing, and so on. In this regard, the real-time retail price varies hourly to reflect wholesale price changes, as well as plays a key role in economical operation and efficient energy management for both MGO and consumers.

In a competitive electricity retail market, consumers are no longer just price takers, and instead they may have impacts on the clearance in an electricity retail market. Only considering economic aspects of retailers or consumers on setting the real-time price (RTP) of electricity is not fair for the other side. The Stackelberg game, being superbly efficient for designing the RTP in the microgrid with a leader-follower structure, is widely used to determine the real-time retail price of electricity recently [5, 6].

A commercial building (CB), as one of major power consumers, usually controls the loads therein in a centralised manner, and thus should be regarded as effective and promising DR resources in the microgrid [7, 8]. However, the reported DR resources of CBs mostly refer to the heating, ventilation and air conditioning (HVAC) system, and the weather uncertainties on DR strategies are usually neglected. This situation motivates us to deeply and comprehensively study the DR model of CBs as well as determine an optimal real-time retail pricing scheme for CBs in a microgrid.

1.2 Literature review

Generally, the HVAC system accounts for most of the energy consumption in CBs [9]. Due to thermal storage characteristics of buildings, the HVAC system usually acts as a DR resource to respond to the RTP of electricity with respecting the indoor temperature comfort levels. In [10], a HVAC system is modelled as a virtual storage and then an optimal coordination dispatch scheme is developed for the HVAC system and ESS. In [11], an experiment is carried out to demonstrate that a HVAC system in CBs is capable of providing a satisfactory frequency regulation without adverse impacts on the indoor climate. Except for keeping the indoor heat balance, a HVAC system also influences the indoor air quality (IAQ) as a result of its circulating indoor and outdoor air [12]. Similar to HVAC systems, lighting systems, which account for a certain portion of power consumption in CBs, could be regarded as curtailable loads with the best use of daylight [13, 14]. However, existing publications have not yet developed DR models with a comprehensive investigation into indoor thermal comfort, IAQ, and lighting conditions. Besides, for economic and environmental benefits, the photovoltaic (PV) panels could be installed on the roof of CBs. Therefore, it is demanding to develop a coordinated power dispatch scheme for HVAC systems, lighting systems and PV outputs for CBs.

Moreover, the DR energy management model is closely related to weather regimes, whose uncertainties could have significant impacts on the power dispatching. In [15], the solar irradiance and outdoor temperature uncertainties are addressed in a solar-assisted HVAC system coupled with a water heating system. However, the effects of correlations among a variety of weather uncertainties on the DR model are neglected, and the accuracy of the results obtained is questionable. Some publications have discussed several methods of solving correlated uncertainties, for example, the Monte–Carlo simulation [16], $2M+1$ point estimate method (PEM) [16], and Latin Hypercube Sampling [17]. Among those simulation methods, $2M+1$ PEM efficiently reduces computational burden and shows great performance for calculating statistical moments of random output quantities [18]. Further, Nataf transformation is employed in [18] to transform the non-normal random variables into normal random variables, which gives an easier access to the weighting factors in PEM. The Nataf transformation based $2M+1$ PEM is thus used to deal with the correlated weather uncertainties in the demand response management (DRM) problem here.

In order to implement the DRM of CBs efficiently, it is critical to make a reasonable RTP signal. Recently, there have been growing interests in adopting the Stackelberg game to model the electricity-trading process between the MGO and consumers for an optimal RTP scheme. In the game, the MGO acts as a leader to determine a RTP scheme with the objective of revenues maximisation while consumers, as followers, respond to RTP for minimisation of the electricity purchasing cost [19, 20]. Ref. [21] uses the non-cooperative Stackelberg game to model grid-to-vehicle energy exchanges between a smart grid and plug-in electric vehicle groups. Ref. [22] models the virtual electricity-trading

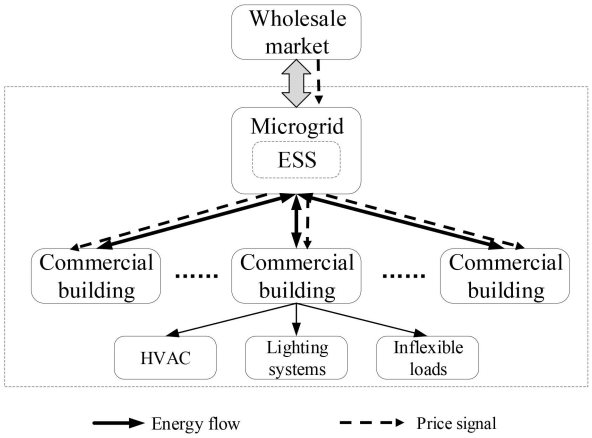

Fig. 1 *System model for the microgrid with commercial buildings*

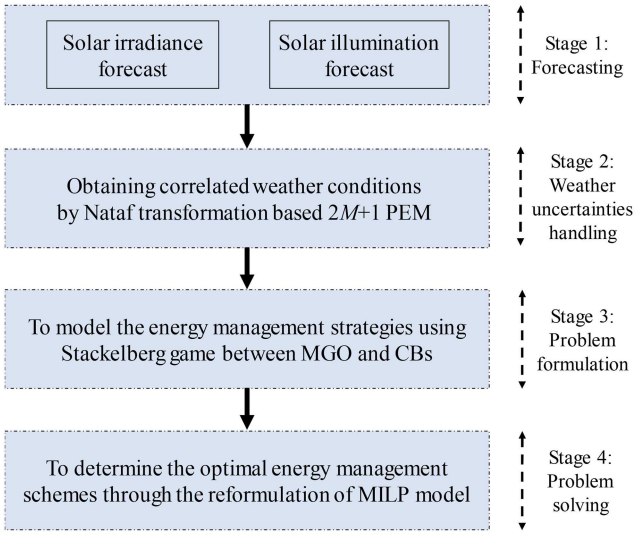

Fig. 2 *Implementation process of the proposed model*

process, in which the energy management centre acts as leader (e.g. a virtual retailer) and offers virtual retail prices to followers (e.g. DR devices). A two-level game is proposed in [4] to describe interactions between multiple utility companies and residential users. A non-cooperative game model is constructed to simulate the interactions among utility companies in the upper level, while an evolutionary game is formulated wherein each user chooses one utility company to buy energy in the lower level. These publications and our work all employ the Stackelberg game to determine an optimal RTP in a microgrid. However, here the followers are specified as CBs, and the lower level problem is modelled with appliance-level details considering the correlated weather uncertainties. This formulation is more practical and accurate.

1.3 Contribution and paper organisation

Based on the given literature review, this paper presents a Stackelberg game-based energy management model for a microgrid and CBs therein. The main contributions of this paper are threefold:

(i) A comprehensive DR-based energy management model for a CB consisting of a HVAC system, a lighting system and PV arrays is developed. The correlation between solar irradiance and illuminance uncertainties, which is simulated by the Nataf transformation-based $2M+1$ PEM with high accuracy and computation speed, is incorporated into the model.
(ii) A bi-level model for the energy management of a microgrid and RTP scheme setting is proposed. At the upper level, the MGO determines the power dispatch and offers the RTP signals to CBs. At the lower level, the CB adjusts its power consumption responding to the RTP signals. The hierarchical interactions between the MGO and CBs are modelled by a Stackelberg game.
(iii) The proposed model is reformulated into a mixed integer linear programming (MILP) problem through three steps: a) McCormick relaxation is employed to deal with bilinear terms in the HVAC DR model; b) the optimality of DR problem in the lower model is denoted by Karush–Kuhn–Tucker (KKT) conditions and big-M disjunctive constraints; c) the bilinear terms in the objective function of the upper model are linearised by using the strong duality theory.

The remainder of this paper is organised as follows. In Section 2, the model description and formulation are introduced. The solution methodology is presented in Section 3. Case studies and numerical results are given in Section 4, followed by the conclusion in Section 5.

2 Model formulation

2.1 Model description

To have a clear and intuitive understanding of the bi-level model, Fig. 1 presents the infrastructure of a microgird with N_{cb} consistent CBs, and Fig. 2 depicts a flowchart of the model implementation process.

(i) *Step 1*: The solar irradiance and illumination are predicted, and the errors modelled by two representative probability distribution functions.
(ii) *Step 2*: The Nataf transformation-based $2M+1$ PEM is applied to simulate the correlated weather conditions which are the input parameters in the DR model of CBs.
(iii) *Step 3*: The energy management problem is modelled by the Stackelberg game, wherein the MGO acts as the leader and CBs the followers..
(iv) *Step 4*: The bilinear terms in the HVAC DR model are dealt with the McCormick relaxation. Then, the KKT conditions, big-M disjunctive constraints and the strong duality theory are successively employed to reformulate the bi-level model into a MILP model. Finally, the optimal energy management scheme is attained.

The framework of Stackelberg game-based energy management bi-level model is presented in Fig. 3 and the detailed descriptions of each entity are stated as follows:

(i) *MGO*: The MGO is an intermediary agent between the wholesale market and consumers. In the wholesale market, the MGO receives wholesale prices and trades with the ISO to balance the supplies and demands. In the retail market, the MGO sets retail prices to guide CBs to manage energy consuming optimally. The microgrid-owned ESS enhances the flexibility and economic performance of the microgrid.
(ii) *CBs*: The CBs, as followers, respond to the retail prices propagated by the MGO considering the weather uncertainties and make full use of PV outputs as well as schedule a HVAC system and lighting systems in a coordinated manner for operation cost minimisation.

As shown in Fig. 3, in the Stackelberg gaming process, MGO acts as the leader, by propagating its strategy (i.e. retail prices ρ_t^{in}) to the followers, that is, the CBs. After receiving the announced price, each follower determines the best power-consumption scheme (i.e. load power P_t^{in}), which is taken as feedback information to the leader. Then, the leader re-optimises its strategy and offers a new real-time retail price of electricity. The interaction process is iterated until every player in the game obtains its most satisfactory results. In other words, the Stackelberg equilibrium is achieved and each player is not willing to deviate from this equilibrium [23]. The corresponding gaming models of the two players are presented with more details in the following sections.

Note that the model to be developed in this work is based on the discrete-event system. Specifically, the operation cycle is divided

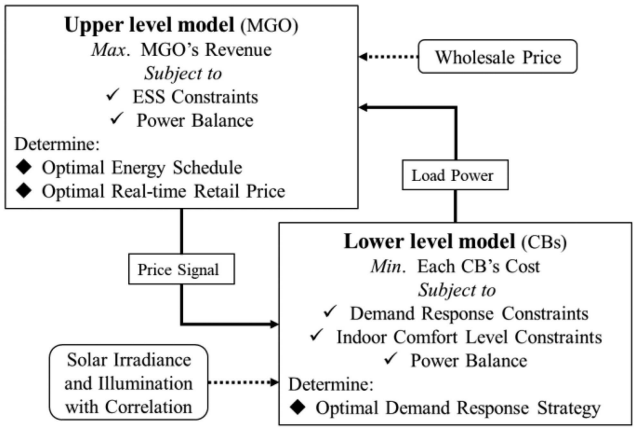

Fig. 3 *Framework of the Stackelberg game based energy management bilevel model*

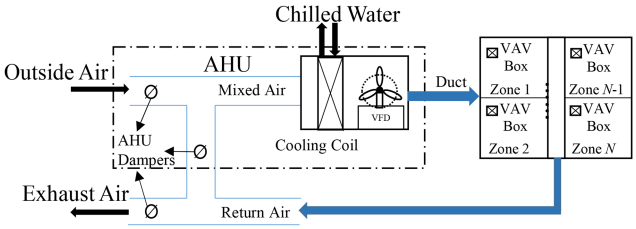

Fig. 4 *Schematic of a typical HVAC system*

into T periods, and the operation state in each period is assumed to remain unchanged. Therefore, the state parameters at the instant t can be used to describe the state during the time interval $(t-1, t)$.

2.2 Model of MGO

The ESS in the microgrid is modelled as follows:

$$S_t = S_{t-1} + \left(\eta_{cha} P_{cha,t} - \frac{P_{dis,t}}{\eta_{dis}}\right) \tag{1}$$

$$0 \le P_{cha,t} \le x_{cha,t} P_{cha}^{max} \tag{2}$$

$$0 \le P_{dis,t} \le (1 - x_{cha,t}) P_{dis}^{max} \tag{3}$$

$$S_{\min} \le S_t \le S_{\max} \tag{4}$$

where (1) represents the changes of the energy storage of ESS between two adjacent periods. Cons. (2) and Cons. (3) impose the upper/lower limits on the charging and discharging power, respectively. Cons. (4) denotes the limits on the ESS capacity.

As a leader in the Stackelberg game, the MGO needs to maximise its profits, and the corresponding optimisation problem is formulated as follows:

$$\max \sum_{t=1}^{T} N_{cb} \rho_t^{in} P_t^{in} - \rho_t^{ws} P_t^{ws} \tag{5}$$

$$\text{s.t.}\,(1) - (4) \tag{6}$$

$$\rho_t^{\min} \le \rho_t^{in} \le \rho_t^{\max} \tag{7}$$

$$\sum_{t=1}^{T} \rho_t^{\text{in}} / T \le \rho_{\text{ave}}^{\text{in}} \tag{8}$$

$$-P_{\max}^{ws} \le P_t^{ws} \le P_{\max}^{ws} \tag{9}$$

$$P_t^{ws} + P_{dis,t} = P_{cha,t} + N_{cb} P_t^{in} \tag{10}$$

where the retail price ρ_t^{in} is the decision variable. For simplicitity, it is assumed that all the CBs share the same load power. The first item in the objective function (5) denotes the income by selling electricity to consumers, and the second item represents the purchasing cost in the wholesale market. Cons. (7) maintains the retail price within the interval $[\rho_t^{\min}, \rho_t^{\max}]$ in each period. Cons. (8) imposes an upper bound on the average value of the retail price sequence to alleviate the market power of MGO [3]. Cons. (9) restricts the range of trading power with the ISO, with positive values indicating purchasing power from the wholesale market, and negative values indicating selling power otherwise. Equation (10) represents the electric power balance in the microgrid.

2.3 Model of CBs

A CB proposed here includes PV, inflexible loads, a HVAC system, and a lighting system. The PV panel realises photoelectric conversion, which is expressed as

$$P_{sol,t} = \tau_{sol}^{ele} A_{ele}^{i} E_t \tag{11}$$

Electric loads are divided into inflexible loads and flexible ones (e.g. a HVAC system and a lighting system), which could respond to the RTP to adjust the power consumption with respecting the corresponding comfort level.

a) The model of a HVAC system

As Fig. 4 shows, a typical commercial HVAC system model consists of an Air Handling Unit (AHU) for the whole building and a set of Variable Air Volume (VAV) boxes in each zone [7]. AHU dampers, a cooling coil, and a Variable Frequency Drive (VFD) are the three main components of the AHU. Returned air from the zones and outside air are mixed by AHU dampers, then the mixed air is cooled down by the cooling coil and further delivered to the VAV box in each zone by the VFD. The damper in a VAV box is used to adjust the rate of the supply air. The refrigeration power of the HVAC system is mainly affected by the refrigeration temperature and the air flow rate, which are considered as the two controllable variables in the model of the HVAC system.

It is assumed that a CB has N zones. For each zone i, the thermal dynamic model is stated as follows:

$$c_{\text{air}} \rho_{\text{air}} V^i \frac{\mathrm{d}\theta_t^i}{\mathrm{d}t} = c_{\text{air}} m_{\text{HVAC},t}^i (\theta_t^{\text{cool}} - \theta_t^i) + B^i(\theta_t^{\text{out}} - \theta_t^i) + Q_{\text{solar},t}^i + Q_{\text{infle},t}^i + Q_{\text{light},t}^i + Q_{\text{crowd},t}^i \tag{12}$$

Compared with other heat resources, the influence of the heat transfer between neighbouring zones is so small and can then be neglected in the above equation. In order to simplify the optimisation problem, the thermal dynamic differential equation can be transformed into the difference equation considering the slow property of heat dissipation process and temperature changes in the building: (see (13)) . The solar radiation heat $Q_{solar,t}^i$ for each zone in the building is calculated as follows:

$$Q_{solar,t}^i = F_{\text{win}}^i E_t S_{\text{she}}^i \tag{14}$$

The lighting system and inflexible loads convert part of electric energy into thermal energy during working process, and accommodate the constraints:

$$c_{\text{air}} \rho_{\text{air}} V^i \frac{\theta_t^i - \theta_{t-1}^i}{\Delta t} = c_{\text{air}} m_{HVAC,t}^i \left(\theta_t^{cool} - \theta_t^i\right) + B^i(\theta_t^{out} - \theta_t^i) + Q_{solar,t}^i + Q_{infle,t}^i + Q_{light,t}^i + Q_{crowd,t}^i \tag{13}$$

$$Q^i_{light,t} = \lambda_{light} P^i_{light,t} \tag{15}$$

$$Q^i_{infle,t} = \lambda_{infle} P^i_{infle,t} \tag{16}$$

The heat dissipation of the crowd includes sensible heat and latent heat, which can be expressed as

$$Q^i_{crowd,t} = n^i_{crowd,t} \phi k q_{sen} + n^i_{crowd,t} \phi q_{lat} \tag{17}$$

In addition to the contributions to the indoor thermal comfort, a HVAC has some impacts on the IAQ. Generally, the CO_2 concentration serves as an index for measuring the IAQ [24]. Similar to the building thermal dynamic process, the CO_2 concentration dynamic difference model can be expressed as:

$$\rho_{\text{air}} V^i \frac{C^i_t - C^i_{t-1}}{\Delta t} = m^i_{HVAC,t}\left(C^{mix}_t - C^i_t\right) + C^i_{crowd,t} \tag{18}$$

where $C^{mix}_t = \delta \dfrac{\sum_{i=1}^{N} m^i_{HVAC,t} C^i_t}{\sum_{i=1}^{N} m^i_{HVAC,t}} + (1-\delta) C^{out}_t$ is the mixed CO_2 concentration; $\delta \in [0,1]$ represents the damper position in the AHU.

For each zone, the indoor thermal comfort range and air quality range are, respectively, constrained by:

$$\theta_{\min} \le \theta^i_t \le \theta_{\max} \tag{19}$$

$$C_{\min} \le C^i_t \le C_{\max} \tag{20}$$

The power consumption associated with a HVAC system broadly results from the cooling coil and the supply fan [11, 14, 25], which can be expressed as

$$P_{\text{HVAC},t} = P_{\text{coil},t} + P_{\text{fan},t} \tag{21}$$

$$P_{\text{coil},t} = \frac{c_{\text{air}}\left(\sum_{i=1}^{N} m^i_{HVAC,t}\right)\left(\theta^{mix}_t - \theta^{cool}_t\right)}{\eta COP} \tag{22}$$

$$P_{\text{fan},t} = k_2 \left(\sum_{i=1}^{N} m^i_{HVAC,t}\right)^2 + k_1 \sum_{i=1}^{N} m^i_{HVAC,t} + k_0 \tag{23}$$

where $\theta^{mix}_t = \delta \dfrac{\sum_{i=1}^{N} m^i_{HVAC,t} \theta^i_t}{\sum_{i=1}^{N} m^i_{HVAC,t}} + (1-\delta)\theta^{out}_t$ represents the temperature of mixed air before entering the cooling coil. The input variables of the CB HVAC system in each period are denoted by $u_t = \left(m^1_{HVAC,t}, m^2_{HVAC,t}, \ldots, m^N_{HVAC,t}, \theta^{cool}_t\right)$, which accommodate the following constraints:

$$m^{\min}_{HVAC} \le m^i_{HVAC,t} \le m^{\max}_{HVAC} \tag{24}$$

$$\sum_{i=1}^{N} m^i_{HVAC,t} \le M^{\max}_{HVAC} \tag{25}$$

$$\theta^{cool}_{\min} \le \theta^{cool}_t \le \theta^{cool}_{\max} \tag{26}$$

Further, assume that N zones have the same system parameters, thus (18) is simplified into:

$$\rho_{\text{air}} V^i \frac{C^i_t - C^i_{t-1}}{\Delta t} = m^i_{HVAC,t}(1-\delta)\left(C^{out}_t - C^i_t\right) + C^i_{crowd,t} \tag{27}$$

Similarly, (22) is simplified into:

$$P_{\text{coil},t} = \frac{c_{\text{air}} N m^i_{HVAC,t}\left(\delta\theta^i_t + (1-\delta)\theta^{out}_t - \theta^{cool}_t\right)}{\eta COP} \tag{28}$$

as well as (23) is:

$$P_{\text{fan},t} = k_2 N^2 {m^i_{HVAC,t}}^2 + k_1 N m^i_{HVAC,t} + k_0 \tag{29}$$

b) The model of a lighting system

The zonal illumination could be provided by the building lighting system and solar illumination. Given that the CB concerned is able to make the best of daylight, the lighting system could act as curtailable loads to participate in DRM. Under the retail price signal, the zonal illumination is assumed to stay within a certain range responding to the RTP [13, 26]. Thus, the lighting illumination needed at time t is expressed as

$$IL_{\max} \ge IL^i_{in,t} + IL_{out,t} \ge IL_{\min} \tag{30}$$

The corresponding electric power of a lighting system is modelled as

$$IL^i_{in,t} R_{light} F^i_{in} = P^i_{light,t} \tag{31}$$

2.3.1 Energy optimal management model: To have a coordinated schedule of DR resources, the CB aims at minimising its costs of purchasing electricity according to RTP signals. The optimal energy management model can be expressed as

$$\min \sum_{t=1}^{T} \rho^{in}_t P^{in}_t \tag{32}$$

$$\text{s.t.}\ (11) - (31) \tag{33}$$

$$-P^{in}_{\max} \le P^{in}_t \le P^{in}_{\max} \tag{34}$$

$$P^{in}_t + P_{sol,t} = \sum_{i=1}^{N} P^i_{infle,t} + \sum_{i=1}^{N} P^i_{light,t} + P_{\text{HVAC},t} \tag{35}$$

where Const. (34) restricts the exchange power between the MGO and consumers, with the positive value indicating the consumer purchasing power from the retailer, and the negative value indicating the consumer selling power. Const. (35) describes the electric power balance in the CB.

2.4 Correlated solar irradiance and illuminance uncertainties

As for the lower level problem, the solar irradiance has some impacts on the HVAC refrigeration output and PV output power while the solar illuminance influences the lighting system loads. Generally, there is a strong positive correlation between the solar irradiance and illuminance. Conventional independent sampling of above two parameters limits the practical application of the model. Here, the Nataf transformation-based $2M+1$ PEM is applied to deal with the correlated uncertainties.

2.4.1 Nataf transformation: The Nataf transformation is employed to transform the input random variables into independent standard normal variables as a basis input for the $2M+1$ PEM regardless of how the input random variables are distributed.

Supposing a system consisting of M correlated input random variables $I=[I_1, I_2, \ldots, I_M]$ with any arbitrary type of marginal distributions, the input variables can be transformed into M dependent standard normal vectors $Z=[Z_1, Z_2, \ldots, Z_M]$ as follows [27]:

$$Z_i = \Phi_i^{-1}(F_i(I_i)) \tag{36}$$

where F_i denotes the cumulative distribution function (CDF) of I_i, Φ_i denotes the CDF of Z_i. By reverting (36), I could be derived from Z:

$$I_i = F_i^{-1}(\Phi_i(Z_i)) \tag{37}$$

The correlation matrix C_I of the correlated input variables I and the corresponding correlation matrix C_Z of the dependent standard normal variables Z can be, respectively, expressed as:

$$C_I = \begin{bmatrix} 1 & \rho_{12} & \cdots & \rho_{1m} \\ \rho_{21} & 1 & \cdots & \rho_{2m} \\ \vdots & \vdots & \ddots & \vdots \\ \rho_{m1} & \rho_{m2} & \cdots & 1 \end{bmatrix} \tag{38}$$

$$C_Z = \begin{bmatrix} 1 & \rho'_{12} & \cdots & \rho'_{1m} \\ \rho'_{21} & 1 & \cdots & \rho'_{2m} \\ \vdots & \vdots & \ddots & \vdots \\ \rho'_{m1} & \rho'_{m2} & \cdots & 1 \end{bmatrix} \tag{39}$$

where ρ_{ij} can be obtained based on the historical data and ρ'_{ij} can be transformed from ρ_{ij} according to the specific function relationship given in [28].

The matrix C_z is symmetric by definition, and thus can be decomposed by the Cholesky decomposition:

$$C_z = LL^T \tag{40}$$

where L is a lower triangular matrix whose inverse matrix B is used in (41) to get the independent standard normal vectors S:

$$S = BZ \tag{41}$$

Thus far, the Nataf transformation is built completely.

2.4.2 2M + 1 PEM: The $2M+1$ PEM developed in [29] concentrates first four central moments of each input random variable I_i, namely its mean, variance, skewness, and kurtosis, into three concentrations. The kth concentration ($I_{i,k}$, $\omega_{i,k}$) of I_i is defined as a pair of a location $I_{i,k}$ and weight coefficient $\omega_{i,k}$. Assuming that Y represents the response function of the model, the location is the kth value of variable at which the response function Y is evaluated, while the weight coefficient accounts for the relative importance of this evaluation in the final output result [30].

The location $I_{i,k}$ is given by:

$$I_{i,k} = \mu_i + \xi_{i,k}\sigma_i \quad \mathrm{i} = 1, 2, \ldots, \mathrm{M}, \quad \mathrm{k} = 1{:}3 \tag{42}$$

where μ_i and σ_i are the mean and standard deviation of I_i, respectively. $\xi_{i,k}$ is the standard location [29, 31]:

$$\xi_{i,k} = \begin{cases} \dfrac{\lambda_{i,3}}{2} + (-1)^{3-k}\sqrt{\lambda_{i,4} - \dfrac{3}{4}\lambda_{i,3}^2} & \mathrm{k} = 1, 2 \\ 0 & \mathrm{k} = 3 \end{cases} \tag{43}$$

where $\lambda_{i,3}$ and $\lambda_{i,4}$ are coefficients of skewness and kurtosis, respectively, and are stated as follows:

$$\begin{cases} \lambda_{i,3} = E\left[(I_i - \mu_i)^3\right]/\sigma_i^3 \\ \lambda_{i,4} = E\left[(I_i - \mu_i)^4\right]/\sigma_i^4 \end{cases} \tag{44}$$

The weight coefficient $\omega_{i,k}$ can calculated by:

$$\omega_{i,k} = \begin{cases} \dfrac{(-1)^{3-k}}{\xi_{i,k}(\xi_{i,1} - \xi_{i,2})} & \mathrm{k} = 1, 2 \\ \dfrac{1}{M} - \dfrac{1}{\lambda_{i,4} - \lambda_{i,3}^2} & \mathrm{k} = 3 \end{cases} \tag{45}$$

Then, the result O of the model can be expressed as:

$$O = \omega_0 Y(\mu_1, \mu_2, \cdots \mu_i, \cdots, \mu_M) + \sum_{i=1}^{M}\sum_{k=1}^{3} \omega_{i,k} Y(\mu_1, \mu_2, \cdots I_{i,k}, \cdots, \mu_M) \tag{46}$$

To sum up, the procedures for the Nataf transformation-based $2M + 1$ PEM are stated as follows.

(i) For independent standard normal variables, mean, variance, skewness, and kurtosis are set as 0, 1, 0, and 3, respectively. Locations and weight coefficients could be calculated according to Eqns. (42)–(45).
(ii) The locations of independent standard normal variables could be transformed into those of input random variables according to Eqns. (36)–(41).
(iii) The result of the model can be obtained by weight coefficients of independent standard normal variables in step 1 and locations of input random variables in step 2.

3 Solution methodology

Quite a few methods are available for solving a multi-objective optimisation problem. The Multi-Objective Particle Swarm Optimisation (MOPSO) algorithm is employed to obtain the optimal solution set of the optimisation problem in [32, 33], and the membership function-based trade-off solution is then taken as the final solution. Nevertheless, the solution such attained is just an approximate optimal one.

The multi-objective optimisation problem presented here is essentially a typical bi-level model, and is commonly reformulated as a mixed-integer linear programming (MILP) model using KKT conditions or dual problems to represent the optimality of the lower level problem [34, 35]. To handle the bilinear items in the lower level problem, the McCormick relaxation is first employed to realise the linearisation of the constraints in the lower level model. Compared with heuristic algorithms, the proposed algorithm can converge to the optimal solution in a finite number of steps and can reach the equilibrium point efficiently.

Here, the proposed bi-level model is reformulated into a standard MILP problem which can be solved efficiently by off-the-shelf commercial solvers.

3.1 McCormick relaxation for HVAC model

The McCormick relaxation replaces each bilinear term or quadratic term with an auxiliary variable and additional four sets of constraints [36]. In HVAC model, there exist three bilinear terms, for example, $m^i_{HVAC,t}\theta^{cool}_t$, $m^i_{HVAC,t}\theta^i_t$ and $m^i_{HVAC,t}C^i_t$, and one quadratic term $m^{i2}_{HVAC,t}$, which can be, respectively, replaced by $\pi^i_{\mathrm{HVACcool},t}$, $\pi^i_{\mathrm{HVACin},t}$ and $\pi^i_{\mathrm{HVACco2},t}$, $\pi^i_{HVAC2,t}$. Therefore, (13), (27) and (28), (29) can be reformulated as: (see (47))

$$\rho_{\mathrm{air}}V^i\frac{C^i_t - C^i_{t-1}}{\Delta t} = m^i_{\mathrm{HVAC},t}(1-\delta)C^{\mathrm{out}}_t - (1-\delta)\pi^i_{\mathrm{HVACco2},t} + C^i_{\mathrm{crowd},t} \tag{48}$$

$$c_{\mathrm{air}}\rho_{\mathrm{air}}V^i\frac{\theta^i_t - \theta^i_{t-1}}{\Delta t} = c_{\mathrm{air}}\left(\pi^i_{\mathrm{HVACcool},t} - \pi^i_{\mathrm{HVACin},t}\right) + B^i\left(\theta^{out}_t - \theta^i_t\right) + Q^i_{solar,t} + Q^i_{infle,t} + Q^i_{light,t} + Q^i_{crowd,t} \tag{47}$$

$$P_{\text{coil},t}=\frac{c_{\text{air}}N\left(\delta\pi^{i}_{\text{HVACin},t}+(1-\delta)m^{i}_{HVAC,t}\theta^{out}_{t}-\pi^{i}_{\text{HVACcool},t}\right)}{\eta COP} \quad (49)$$

$$P_{\text{fan},t}=k_2N^2m^{i}_{HVAC2}+k_1Nm^{i}_{HVAC,t}+k_0 \quad (50)$$

The constraints for auxiliary variables are formulated as follows:

$$\begin{cases}\pi^{i}_{\text{HVACcool},t}\geq m^{i}_{HVAC,t}\theta^{cool}_{\min}+m^{\min}_{HVAC}\theta^{cool}_{t}-m^{\min}_{HVAC}\theta^{cool}_{\min}\\ \pi^{i}_{\text{HVACcool},t}\geq m^{i}_{HVAC,t}\theta^{cool}_{\max}+m^{\max}_{HVAC}\theta^{cool}_{t}-m^{\max}_{HVAC}\theta^{cool}_{\max}\\ \pi^{i}_{\text{HVACcool},t}\leq m^{i}_{HVAC,t}\theta^{cool}_{\min}+m^{\max}_{HVAC}\theta^{cool}_{t}-m^{\max}_{HVAC}\theta^{cool}_{\min}\\ \pi^{i}_{\text{HVACcool},t}\leq m^{i}_{HVAC,t}\theta^{cool}_{\max}+m^{\min}_{HVAC}\theta^{cool}_{t}-m^{\min}_{HVAC}\theta^{cool}_{\max}\end{cases} \quad (51)$$

$$\begin{cases}\pi^{i}_{\text{HVACin},t}\geq m^{i}_{HVAC,t}\theta_{\min}+m^{\min}_{HVAC}\theta^{i}_{t}-m^{\min}_{HVAC}\theta_{\min}\\ \pi^{i}_{\text{HVACin},t}\geq m^{i}_{HVAC,t}\theta_{\max}+m^{\max}_{HVAC}\theta^{i}_{t}-m^{\max}_{HVAC}\theta_{\max}\\ \pi^{i}_{\text{HVACin},t}\leq m^{i}_{HVAC,t}\theta_{\min}+m^{\max}_{HVAC}\theta^{i}_{t}-m^{\max}_{HVAC}\theta_{\min}\\ \pi^{i}_{\text{HVACin},t}\leq m^{i}_{HVAC,t}\theta_{\max}+m^{\min}_{HVAC}\theta^{i}_{t}-m^{\min}_{HVAC}\theta_{\max}\end{cases} \quad (52)$$

$$\begin{cases}\pi^{i}_{\text{HVACco2},t}\geq m^{i}_{HVAC,t}C_{\min}+m^{\min}_{HVAC}C^{i}_{t}-m^{\min}_{HVAC}C_{\min}\\ \pi^{i}_{\text{HVACco2},t}\geq m^{i}_{HVAC,t}C_{\max}+m^{\max}_{HVAC}C^{i}_{t}-m^{\max}_{HVAC}C_{\max}\\ \pi^{i}_{\text{HVACco2},t}\leq m^{i}_{HVAC,t}C_{\min}+m^{\max}_{HVAC}C^{i}_{t}-m^{\max}_{HVAC}C_{\min}\\ \pi^{i}_{\text{HVACco2},t}\leq m^{i}_{HVAC,t}C_{\max}+m^{\min}_{HVAC}C^{i}_{t}-m^{\min}_{HVAC}C_{\max}\end{cases} \quad (53)$$

$$\begin{cases}\pi^{i}_{\text{HVAC2},t}\geq 2m^{\min}_{HVAC}m^{i}_{HVAC,t}-{m^{\min}_{HVAC}}^{2}\\ \pi^{i}_{\text{HVAC2},t}\geq 2m^{\max}_{HVAC}m^{i}_{HVAC,t}-{m^{\max}_{HVAC}}^{2}\\ \pi^{i}_{\text{HVAC2},t}\leq m^{i}_{HVAC,t}m^{\min}_{HVAC}+m^{\max}_{HVAC}m^{i}_{HVAC,t}-m^{\max}_{HVAC}m^{\min}_{HVAC}\end{cases} \quad (54)$$

3.2 KKT conditions of the lower model

When the retail prices are fixed, the lower model would be transformed into a linear problem, and its optimality can be represented by KKT conditions [3]. Generally, given an optimisation model P_1:

$$P_1:\begin{cases}\min \mathrm{f}(\boldsymbol{x})\\ \mathrm{s.t.}\ \boldsymbol{h}(\boldsymbol{x})\leq\boldsymbol{b}\\ \boldsymbol{g}(\boldsymbol{x})=\boldsymbol{d}\end{cases} \quad (55)$$

Then, the corresponding Lagrange function $\boldsymbol{\Gamma}(x)$ and KKT conditions are formulated as follows:

$$\begin{cases}\boldsymbol{\Gamma}(\boldsymbol{x})=f(\boldsymbol{x})+\boldsymbol{\mu}^T[\boldsymbol{h}(\boldsymbol{x})-\boldsymbol{b}]+\boldsymbol{\lambda}^T[\boldsymbol{g}(\boldsymbol{x})-\boldsymbol{d}]\\ \dfrac{\mathrm{d}f(x^*)}{\mathrm{d}x}+\left(\dfrac{\partial\boldsymbol{h}(x^*)}{\partial x}\right)^T\boldsymbol{\mu}+(\dfrac{\partial\boldsymbol{g}(x^*)}{\partial x})^T\boldsymbol{\lambda}=0\\ \boldsymbol{\mu}^T[\boldsymbol{h}(x^*)-\boldsymbol{b}]=0\\ \boldsymbol{\mu}\geq 0\end{cases} \quad (56)$$

where $\boldsymbol{\mu}$ is the vector of dual variables of $\boldsymbol{h}(\boldsymbol{x})$, $\boldsymbol{\lambda}$ is the vector of dual variables of $\boldsymbol{g}(\boldsymbol{x})$, $x^*$is the optimum of P_1. In the lower level of our model, Consts. (19)–(20), (24)–(26), (30), (34), (51)–(54) are the inequality constraints, and (21), (31), (35), (47)–(50) are the equality constraints. All the above constraints need to be incorporated into KKT conditions.

The complementary slack constraints in (56) could be linearised into disjunctive constraints (57) using Fortuny–Amat transformation [37]:

$$\begin{cases}0\leq\boldsymbol{\mu}\leq Mz\\ 0\leq\boldsymbol{b}-\boldsymbol{h}(x^*)\leq M(1-z)\end{cases} \quad (57)$$

where M is a positive constant and big enough to avoid a smaller boundary on the original and the dual variables. z is an auxiliary binary variables vector.

3.3 Linearising the bilinear item in objective function (58)

According to the strong dual theory, the objective value of a linear programming problem is equal to its dual problem at the optimal solution. Thus, the bilinear item $\rho^{in}_{t}P^{in}_{t}$ in objective function (5) could be represented by (see (58)) .

4 Case studies and numerical results

The microgrid with three medium-sized office buildings is employed to demonstrate the features of the proposed model. Each office building has eight zones. The hourly retail price is assumed to be from 0.6 to 1.3 times the wholesale price at the corresponding period, and the upper bound of average retail price is assumed to be 2.6 ¢ /kW. The wholesale price is taken from the PJM website [38]. The correlation matrix C_I for solar irradiance and illuminance is assumed as $\begin{bmatrix}1 & 0.7\\ 0.7 & 1\end{bmatrix}$ and their forecast values are given in Fig. 5. It is assumed that the forecast values of solar irradiance are normally distributed with a variance of 0.6 and solar illuminance is characterised by a Rayleigh distribution with a variance of 0.6. The correlation matrix C_Z of the dependent standard normal variables transformed from C_I is $\begin{bmatrix}1 & 0.7098\\ 0.7098 & 1\end{bmatrix}$.

The area of PV array at the roof of each CB is 200 m2, and the PV generation efficiency is set as 0.8. The HVAC system

$$\begin{aligned}&-\rho^{\text{in}}_{t}P^{\text{in}}_{t}=\\ &(c_{\text{air}}\rho_{\text{air}}V^{i}\theta^{i}_{0}+B^{\text{i}}\theta^{\text{out}}_{1}+Q^{i}_{\text{solar},1}+Q^{i}_{infle,1}+Q^{i}_{\text{crowd},1})\lambda_{4,1}+(\rho_{\text{air}}V^{i}C^{i}_{0}+C^{i}_{\text{crowd},t})\lambda_{5,1}\\ &+\sum_{t=2}^{24}\{(B^{\text{i}}\theta^{\text{out}}_{t}+Q^{i}_{\text{solar},t}+Q^{i}_{infle,t}+Q^{i}_{\text{crowd},t})\lambda_{4,t}+(C^{i}_{\text{crowd},t})\lambda_{5,t}\}\\ &\quad\Big\{(\sum_{i=1}^{N}P^{i}_{\text{infle},t}-P_{\text{sol},t})\lambda_{3,t}+k_0\lambda_{7,t}-m^{\min}_{\text{HVAC}}\mu_{1,t}+m^{\max}_{\text{HVAC}}\mu_{2,t}+M^{\max}_{\text{HVAC}}\mu_{3,t}\\ &\quad-\theta_{\min}\mu_{4,t}+\theta_{\max}\mu_{5,t}-\theta^{\text{cool}}_{\min}\mu_{6,t}+\theta^{\text{cool}}_{\max}\mu_{7,t}-C_{\min}\mu_{8,t}+C_{\max}\mu_{9,t}+(IL_{\max}-IL_{\text{out},t})\mu_{10,t}+(IL_{\text{out},t}-IL_{\min})\mu_{11,t}\\ &+\sum_{t=1}^{24}+P^{\text{in}}_{\max}\mu_{12,t}+P^{\text{in}}_{\max}\mu_{13,t}+m^{\text{min2}}_{\text{HVAC}}\mu_{14,t}+m^{\text{max2}}_{\text{HVAC}}\mu_{15,t}-m^{\max}_{\text{HVAC}}m^{\min}_{\text{HVAC}}\mu_{16,t}\\ &\quad+m^{\min}_{\text{HVAC}}\theta^{\text{cool}}_{\min}\mu_{17,t}+m^{\max}_{\text{HVAC}}\theta^{\text{cool}}_{\max}\mu_{18,t}-m^{\max}_{\text{HVAC}}\theta^{\text{cool}}_{\min}\mu_{19,t}-m^{\min}_{\text{HVAC}}\theta^{\text{cool}}_{\max}\mu_{20,t}\\ &\quad+m^{\min}_{\text{HVAC}}\theta_{\min}\mu_{21,t}+m^{\max}_{\text{HVAC}}\theta_{\max}\mu_{22,t}-m^{\max}_{\text{HVAC}}\theta_{\min}\mu_{23,t}-m^{\min}_{\text{HVAC}}\theta_{\max}\mu_{24,t}\\ &\quad+m^{\min}_{\text{HVAC}}C_{\min}\mu_{25,t}+m^{\max}_{\text{HVAC}}C_{\max}\mu_{26,t}-m^{\max}_{\text{HVAC}}C_{\min}\mu_{27,t}-m^{\min}_{\text{HVAC}}C_{\max}\mu_{28,t}\Big\}\end{aligned} \quad (58)$$

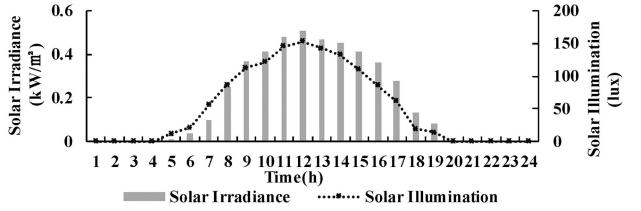

Fig. 5 *Solar irradiance and illumination of a typical summer day*

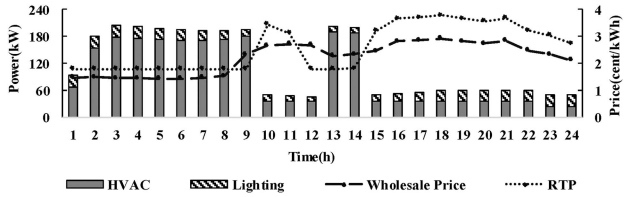

Fig. 6 *Daily power schedules of the office building in Mode 1*

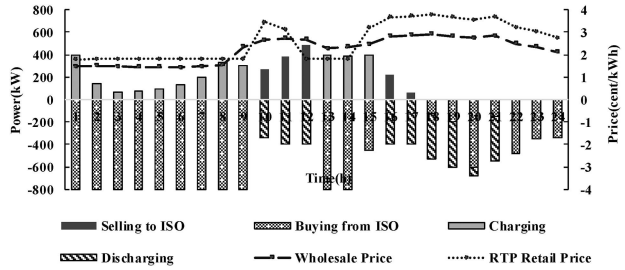

Fig. 7 *Daily power schedules of the MGO in Mode 1*

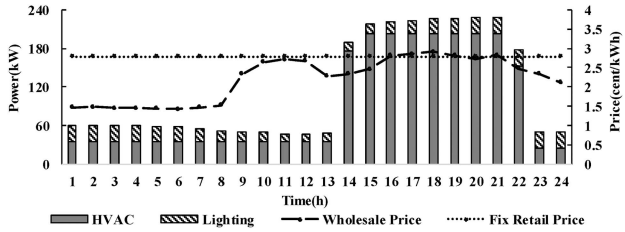

Fig. 8 *Daily power schedules of the office building in Mode 2*

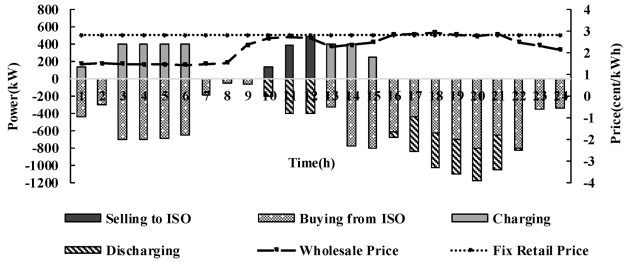

Fig. 9 *Daily power schedules of the MGO in Mode 2*

parameters are adapted from [12, 39]. The generation rate of CO_2 is 0.3L/s/person, and indoor permissible CO_2 concentration ranges from 0.3 to 0.85 [12]. The comfortable indoor temperature is assumed to be within [22°C, 24.5°C] with additional system parameters presented in Table 1.

4.1 Economic analysis and energy management results comparison under different pricing models

To analyse the performance of the proposed model, the following three pricing models are applied.

(i) Mode 1: The proposed Stackelberg game-based RTP is employed. CBs manage loads to respond to the RTP.
(ii) Mode 2: The fixed retail price is employed. CBs have no incentives to adjust load demands.

Table 1 System parameters

Parameter	Value	Parameter	Value
$P^{in}_{\max}$	500	B	0.965
P^{ISO}_{max}	800	F_{win}	170
P^{max}_{cha}	400	S_{she}	0.3
P^{max}_{dis}	400	λ_{light}	0.9
$S_{\max}$	2200	λ_{infle}	0.3
$S_{\min}$	80	ϕ	0.9
c_{air}	1.005	k	0.05
ρ_{air}	1.29	q_{sen}	0.065
V	800	q_{lat}	0.11746

Table 2 Comparison of revenues attained by MGO and power purchasing costs of a CB under three modes

Mode	Revenues of MGO/$	Power purchasing costs of a CB/$
mode 1	77.312	85.715
mode 2	70.449	96.237
mode 3	72.815	87.618

(iii) Mode 3: The TOU pricing is employed. CBs manage loads to respond to TOU prices.

Mode 1 represents the proposed energy management model; Mode 2 represents the situation without implementation of DRM; and Mode 3 represents a definite retail price scheme. Daily revenue of MGO and daily payment of each CB under these three pricing models are listed in Table 2. In the case without implementing DR strategies, Mode 2 is the least economical, in which MGO gains the least revenues and CBs pay most for purchasing electricity. Compared with Mode 2 and Mode 3, the revenue of MGO in Mode 1 slightly increases, whereas the purchasing electricity cost for the CB is yet the least, and this shows that the proposed model attains a win-win solution for both MGO and consumers.

In order to have an intuitive understanding of the proposed energy management schemes, the power scheduling details of Mode 1 and Mode 2 are shown in Figs. 6–9. With a comprehensive consideration of electricity prices and load schedules in Figs. 6 and 7, it is notable that in Mode 1, MGO prefers to lower retail prices in the midnight and early hours of the morning, but raises retail prices in other periods, which could facilitate consumers to adjust power consumption efficiently.

As observed from Fig. 6, in the CBs side, the HVAC system is active in responding to the RTP in Mode 1, with the tendency of working in low retail price periods to reduce costs. Fig. 10 shows the main heat power in the CB in Mode 1. During daylight, there is more solar irradiance, indoor heat sources, and higher outdoor temperature, all speeding up the rise of indoor temperature and further increasing HVAC loads. However, under the guidance of retail price signals, the HVAC system works more in early hours of the morning to precool the zones, and thus could relieve the electricity demands of high retail prices during the day. Besides, it is in the consumers' best interest to sell the surplus of PV generation to MGO for more benefits. In contrast, Fig. 8 indicates that CBs have no ability to shift loads to low retail price periods in Mode 2. Hence, the HVAC system mainly works during high retail price periods without bringing economic benefits for CBs further for the MGO. Compared with Mode 2, it is noteworthy that the proposed pricing model has a slight impact on the lighting system. In both two pricing models, the lighting system, as the curtailable load, effectively uses the daylight to reduce the loads during the day on the premise of meeting the light needs.

In the MGO side, Figs. 7 and 9 indicate that in both modes, the electric energy is purchased by MGO from the wholesale market to charge the ESS or supply to the consumers during low wholesale price periods. During high wholesale price periods, ESS discharges to the wholesale market for revenues increasing. Further in Mode

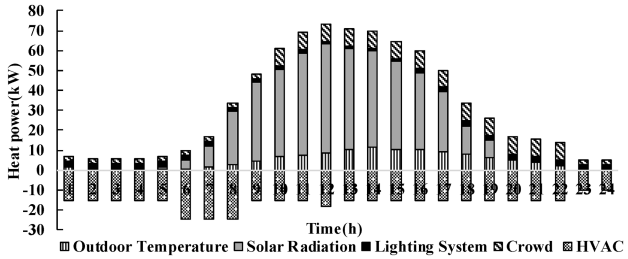

Fig. 10 *Heat power in the commercial building in Mode 1*

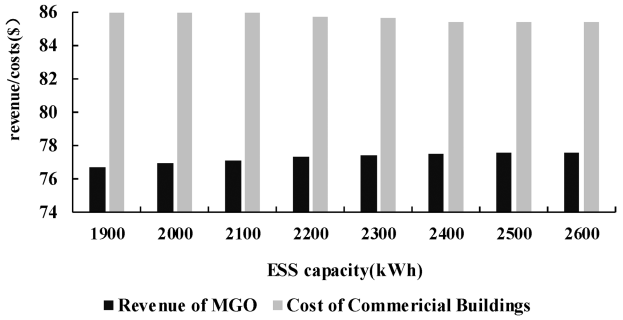

Fig. 11 *Sensitivity analysis of ESS capacity*

1, the CBs implement DR strategies for less purchasing power from the wholesale market during high retail prices period, with the result of revenues increase.

4.2 Analysis of solar irradiance and illuminance uncertainties with correlation

The solar irradiance relates to the HVAC refrigeration output and PV output power while the solar illuminance influences the lighting system loads. In Table 3, the revenues of the MGO and the power purchasing cost of each CB with and without considering the correlations among uncertainties are listed. As observed from Table 3, the results are a bit different in two cases. If the correlation is neglected, it seems that the model outputs better results for CBs, yet causes an overly optimistic illusion for users' actual usage. Therefore, the correlations between solar irradiance and illuminance should be considered for a more practical model.

4.3 Demand response capacity analysis

It is assumed that indoor temperature comfortable range and allowable minimum lighting requirements represent the DR capacity of the HVAC system and the lighting system, respectively. This part shows how demand response capacity influences the energy management.

The numerical results at different indoor comfortable levels are enumerated in Table 4. The larger temperature comfortable range means HVAC loads can be adjusted more flexibly, and thus the costs of purchasing power for consumers become less. However, the limits of the HVAC flow rates and cooling coil temperature alleviate the impacts of DR capacity, resulting that the consumers' costs tend to be stable afterwards. As for the MGO, larger HVAC DR capacity contributes to a more flexible energy scheduling in the microgrid, and theoretically, it would be beneficial to the MGO's revenue to a certain extent. However, the situations appear where a smaller DR capacity causes more MGO's revenues. This is because consumer's purchasing power costs are the main stream of MGO's revenue, and when the costs go up too much, the revenues would most likely increase.

In Table 5, it shows that larger DR capacity of lighting system can be propitious to both MGO and consumers. As the allowable minimum lighting decreases, the revenues of MGO increase while the costs of CBs decline gradually. This is reasonable because the lower allowable minimum lighting allows the CB to curtail more lighting power at the peak price periods for cost saving. Meanwhile, the MGO also has the ability to reduce power purchasing from the wholesale market.

Table 3 Comparison of MGO's revenue and CB's power purchasing costs with and without correlations

	Revenues of MGO/$	Power purchasing costs of a CB/$
with correlations	77.312	85.715
without correlations	75.185	66.786

Table 4 Analysis of the HVAC DR capacity

Allowable indoor temperature range/°C	Revenues of MGO/$	Costs of CB/$
24–24.5	81.962	107.710
23–24.5	77.217	86.513
22–24.5	77.312	85.715
22–24.7	73.613	50.032
22–25	73.643	40.534
21–26	73.658	40.525

Table 5 Analysis of the lighting system DR capacity

Allowable minimum lighting conditions/lux	Revenues of MGO/$	Costs of CB/$
300	76.024	90.388
290	76.468	88.920
280	76.760	87.453
270	77.312	85.715
260	78.089	84.565
250	78.993	83.219

4.4 Sensitivity analysis

In this part, the impacts of ESS capacity and maximum average retail price of electricity will be analysed.

For the upper level, as the key device for energy scheduling, the ESS plays an important role in energy optimisation management. As shown in Fig. 11, consistent with the changes in the ESS capacity, the revenues of MGO increase progressively, whereas the cost of the CB for purchasing electricity only decreases in a particularly small range. It is understandable that a larger capacity of ESS facilitates MGO to purchase more electricity at low price periods and avoid peak prices, thus brings more benefits for MGO. It would also indirectly lower the electricity purchasing cost of CBs to a certain extent, as MGO has a relatively lower cost of purchasing electricity from the wholesale electricity market.

The retail price signal is a vital link in Stackelberg game-based energy management. Fig. 12 indicates that as the maximum average retail price of electricity goes up, the revenue of MGO rises since the costs of purchasing electricity by CBs also increase. Interestingly, there is only a slight increase in the purchasing electricity costs by CBs with the increase of the maximum average retail price of electricity, and this means that the proposed model could effectively protect the interests of CBs, at least to some extent. Besides, in order to avoid excessive high costs of electricity for consumers, it is necessary to set an appropriate upper bound on the retail price of electricity in practical applications.

5 Conclusions

This paper proposes a Stackelberg game-based energy management model for a microgrid with CBs. The loads in CBs are divided into inflexible loads and flexible loads such as a HVAC system and a lighting system. The infrastructure of a microgrid with CBs and the model of each component are presented first. Then the Nataf transformation based $2M+1$ PEM is employed to simulate the correlated solar irradiance and illuminance uncertainties. Further, McCormick relaxation is applied to deal with bilinear and quadratic terms. Then, the bilevel model is transformed into a single-level MILP model by KKT conditions and strong dual theory. The performance of the developed model is assessed

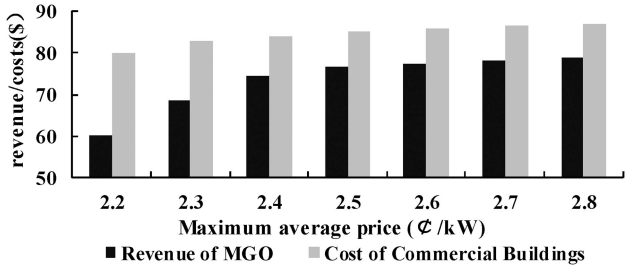

Fig. 12 *Sensitivity analysis of the maximum average retail price of electricity*

through case studies of a microgrid with three office buildings. Simulation results have demonstrated that (i) Stackelberg game based RTP mechanism helps MGO and CBs achieve a win-win solution; (ii) the numerical results are more accurate with the impacts of correlations between solar irradiance and illuminance uncertainties considered; (iii) a larger DR capacity contributes to a more flexible energy management; (iv) the effects of ESS capacity are obvious on MGO power scheduling but inapparent on CBs demand response, while the upper bound of average retail price affects energy management on both MGO and consumers.

The impacts of power network constraints on the Stackelberg game based energy management are not investigated in this paper, and will be examined in our future research efforts.

6 Acknowledgments

This work is jointly supported by National Key Research and Development Program of China (Basic Research Class) (No. 2017YFB0903000), National Natural Science Foundation of China (No. U1509218), and a Science and Technology Project from State Grid Zhejiang Electric Power Company (No. 5211JY17000Q).

7 References

[1] Feng, C., Li, Z., Shaihidehpour, M., *et al.*: 'Decentralized short-term voltage control in active power distribution systems', *IEEE Trans. Smart Grid*, 2018, **9**, (5), pp. 4566–4576

[2] Shen, J., Jiang, C., Liu, Y., *et al.*: 'A microgrid energy management system and risk management under an electricity market environment', *IEEE. Access.*, 2016, **4**, pp. 2349–2356

[3] Wei, W., Liu, F., Mei, S.: 'Energy pricing and dispatch for smart grid retailers under demand response and market price uncertainty', *IEEE Trans. Smart Grid*, 2017, **6**, (3), pp. 1364–1374

[4] Chai, B., Chen, J., Yang, Z., *et al.*: 'Demand response management with multiple utility companies: a two-level game approach', *IEEE Trans. Smart Grid*, 2014, **5**, (2), pp. 722–731

[5] Liu, N., Yu, X., Wang, C., *et al.*: 'Energy sharing management for microgrids with PV prosumers: A stackelberg game approach', *IEEE Trans. Ind. Informat.*, 2017, **13**, (3), pp. 1088–1098

[6] Yang, H., Xie, X., Vasilakos, A.V.: 'Noncooperative and cooperative optimization of electric vehicle charging under demand uncertainty: a robust stackelberg game', *IEEE Trans. Veh. Technol.*, 2016, **65**, (3), pp. 1043–1058

[7] Yu, L., Xie, D., Jiang, T., *et al.*: 'Distributed real-time HVAC control for cost-efficient commercial buildings under smart grid environment', *IEEE Internet Things J.*, 2018, **5**, (1), pp. 44–55

[8] Zhou, Z., Zhao, F., Wang, J.: 'Agent-based electricity market simulation with demand response from commercial buildings', *IEEE Trans. Smart Grid*, 2011, **2**, (4), pp. 580–588

[9] Goddard, G., Klose, J., Backhaus, S.: 'Model development and identification for fast demand response in commercial HVAC systems', *IEEE Trans. Smart Grid*, 2017, **5**, (4), pp. 2084–2092

[10] Hao, H., Wu, D., Lian, J., *et al.*: 'Optimal coordination of building loads and energy storage for power grid and end user services', *IEEE Trans. Smart Grid*, 2018, **9**, (5), pp. 4335–4345

[11] Lin, Y., Barooah, P., Meyn, S., *et al.*: 'Experimental evaluation of frequency regulation from commercial building HVAC systems', *IEEE Trans. Smart Grid*, 2015, **6**, (2), pp. 776–783

[12] Mossolly, M., Ghali, K., Ghaddar, N.: 'Optimal control strategy for a multi-zone air conditioning system using a genetic algorithm', *Energy*, 2009, **34**, (1), pp. 58–66

[13] Brahman, F., Honarmand, M., Jadid, S.: 'Optimal electrical and thermal energy management of a residential energy hub, integrating demand response and energy storage system', *Energy & Buildings*, 2015, **90**, pp. 65–75

[14] Bozchalui, M.C., Hashmi, S.A., Hassen, H., *et al.*: 'Optimal operation of residential energy hubs in smart grids', *IEEE Trans. Smart Grid*, 2012, **3**, (4), pp. 1755–1766

[15] Nguyen, H.T., Nguyen, D.T., Le, L.B.: 'Energy management for households with solar assisted thermal load considering renewable energy and price uncertainty', *IEEE Trans. Smart Grid*, 2015, **6**, (1), pp. 301–314

[16] Morales, J.M., Baringo, L., Conejo, A.J., *et al.*: 'Probabilistic power flow with correlated wind sources', *IET Gener. Transm. Distrib.*, 2010, **4**, (5), pp. 641–651

[17] Chen, Y., Wen, J., Cheng, S.: 'Probabilistic load flow method based on nataf transformation and latin hypercube sampling', *IEEE Trans. Sustain. Energy*, 2013, **4**, (2), pp. 294–301

[18] Li, X., Zhang, X., Wu, L., *et al.*: 'Transmission line overload risk assessment for power systems with wind and load-power generation correlation', *IEEE Trans. Smart Grid*, 2015, **6**, (3), pp. 1233–1242

[19] Meng, F.L., Zeng, X.J.: 'A stackelberg game-theoretic approach to optimal real-time pricing for the smart grid', *Soft Computing*, 2013, **17**, (12), pp. 2365–2380

[20] Maharjan, S., Zhu, Q., Zhang, Y., *et al.*: 'Dependable demand response management in the smart grid: a stackelberg game approach', *IEEE Trans. Smart Grid*, 2013, **4**, (1), pp. 120–132

[21] Tushar, W., Saad, W., Poor, H.V., *et al.*: 'Economics of electric vehicle charging: A game theoretic approach', *IEEE Trans. Smart Grid*, 2012, **3**, (4), pp. 1767–1778

[22] Yu, M., Hong, S.H.: 'A real-time demand-response algorithm for smart grids: A stackelberg game approach', *IEEE Trans. Smart Grid*, 2016, **7**, (2), pp. 879–888

[23] Lu, T., Wang, Z., Wang, J., *et al.*: 'A data-driven stackelberg market strategy for demand response-enabled distribution systems', *IEEE Trans. Smart Grid*, DOI: 10.1109/TSG.2018.2795007

[24] Yang, R., Wang, L.: 'Multi-zone building energy management using intelligent control and optimization', *Sustainable Cities & Society*, 2013, **6**, (1), pp. 16–21

[25] Ma, Y., Matuško, J., Borrelli, F.: 'Stochastic model predictive control for building HVAC systems: complexity and conservatism', *IEEE Trans. Control Syst. Technol.*, 2014, **23**, (1), pp. 101–116

[26] Shang, C., Srinivasan, D., Reindl, T.: 'Joint generation and multiple demand scheduling in off-grid buildings'. IEEE Int. Conf. on Building Efficiency and Sustainable Technologies., Singapore, August-September, 2015, pp. 50–55

[27] Andervazh, M.R., Javadi, S.: 'Emission-economic dispatch of thermal power generation units in the presence of hybrid electric vehicles and correlated wind power plants', *IET Gener. Transm. Distrib.*, 2017, **11**, (9), pp. 2232–2243

[28] Liu, P.L., Der Kiureghian, A.: 'Multivariate distribution models with prescribed marginals and covariances', *Probabilistic Eng. Mech.*, 1986, **1**, (2), pp. 105–112

[29] Hong, H.P.: 'An efficient point estimate method for probabilistic analysis', *Reliab. Eng. Syst. Saf.*, 1998, **59**, (3), pp. 261–267

[30] Morales, J.M., Perez-Ruiz, J: 'Point estimate schemes to solve the probabilistic power flow', *IEEE Trans. Power Syst.*, 2007, **22**, (4), pp. 1594–1601

[31] Evangelopoulos, V.A., Georgilakis, P.S.: 'Optimal distributed generation placement under uncertainties based on point estimate method embedded genetic algorithm', *IET Gener. Transm. Distrib.*, 2014, **8**, (3), pp. 389–400

[32] Baghaee, H.R., Mirsalim, M., Gharehpetian, G.B., *et al.*: 'Reliability/cost-based multi-objective pareto optimal design of stand-alone wind/PV/FC generation microgrid system', *Energy*, 2016, **115**, (1), pp. 1022–1041

[33] Baghaee, H.R., Mirsalim, M., Gharehpetian, G.B.: 'Multi-objective optimal power management and sizing of a reliable wind/PV microgrid with hydrogen energy storage using MOPSO', *J. Intell. Fuzzy Syst.*, 2017, **32**, (3), pp. 1753–1773

[34] Fernandez-Blanco, R., Arroyo, J.M., Alguacil, N.: 'Network-constrained day-ahead auction for consumer payment minimization', *IEEE Trans. Power Syst.*, 2014, **29**, (2), pp. 526–536

[35] Arroyo, J.M.: 'Bilevel programming applied to power system vulnerability analysis under multiple contingencies', *IET Gener. Transm. Distrib.*, 2010, **4**, (2), pp. 178–190

[36] Mccormick, G.P.: 'Computability of global solutions to factorable nonconvex programs: Part I - Convex underestimating problems', *Math. Progr.*, 1976, **10**, (1), pp. 147–175

[37] Fortuny-Amat, J., Mccarl, B.: 'A representation and economic interpretation of a two-level programming problem', *J. Oper. Res. Soc.*, 1981, **32**, (9), pp. 783–792

[38] 'Pennsylvania—New Jersey—Maryland', http://www.pjm.com/markets-and-operations/energy.aspx

[39] Hao, H., Corbin, C.D., Kalsi, K., *et al.*: 'Transactive control of commercial buildings for demand response', *IEEE Trans. Power Syst.*, 2017, **32**, (1), pp. 774–783